行政院國家科學委員會專題研究計畫　成果報告

子計畫一：新穎光電材料與奈米結構元件光學性質之研究

(2/2)

計畫類別：整合型計畫
計畫編號：NSC90-2215-E-002-021-
執行期間：90 年 08 月 01 日至 91 年 09 月 30 日
執行單位：國立臺灣大學光電工程學研究所

計畫主持人：詹國禎
共同主持人：林浩雄

報告類型：精簡報告

處理方式：本計畫可公開查詢

中　華　民　國 92 年 5 月 12 日

行政院國家科學委員會專題研究計畫成果報告

新穎光電材料與奈米結構元件之研究(2/2)—
子計畫一：新穎光電材料與奈米結構元件光學性質之研究

計畫編號：NSC 90-2215-E-002-021

執行期限：90 年 8 月 1 日至 91 年 10 月 31 日

主持人：詹國禎　　執行機構及單位名稱：台灣大學光電所

共同主持人：林浩雄　　執行機構及單位名稱：台灣大學電機系

一、中文摘要

在不同溫度下，以光調制反射率光譜及光激發螢光光譜術量測砷化銦鎵/砷化鎵量子點結構的光學特性，此量子點結構樣品表面經由場發射電子掃描顯微術及原子力顯微術量測分析，其量子點面密度約為每平方公分 1×10^{10} 個。在光激發螢光光譜中顯現五個光學躍遷能譜，其中較低的兩個為量子點內能階躍遷，其次為伴隨形成之超薄量子井的躍遷，最高的兩個能階則為砷化鎵位障及緩衝層所產生。從溫度與躍遷能值關係可推論，兩個量子點的躍遷能譜的來源應是兩群由不同銦成分所構成之量子點的最低能態間光學躍遷所造成。

關鍵詞：

Abstract

The optical properties of InGaAs/GaAs quantum dots (QDs) were investigated by temperature-dependent photoluminescence (PL) and photoreflectance (PR) spectroscopies. The surface morphology and structure analysis of InGaAs QDs were also examined and characterized by a field emission scanning electron microscope (SEM) and an atomic force microscope (AFM). The area density of the QDs is on an order of magnitude about 1×10^{10} dots/cm^2. The PL results exhibited 5 major energy peaks, two of which are attributed to InGaAs QDs, one is attributed to the InGaAs wetting layer and the other two are attributed to GaAs band-gap transitions. Two of the low energy features are identified to the optical transitions of the ground state. They were originated from the two kinds of InGaAs QDs which might be formed with slight change of the indium composition. The results of PR measurements which reveal energy features on the high energy side contributed by GaAs is also reported.

Keywords: InGaAs, Quantum dots, Photoluminescence, SEM, AFM

Ⅰ. Introduction

Low dimensional semiconductor systems have been widely studied in many laboratories over the past two decades. These nanostructure materials and devices have attracted considerable attention during the last decade both from fundamental and technological points of view. Self-assembled quantum dots (QDs), one species of the nanoscale structures, provide three-dimensional confinement of

the charge carriers and consequently have a discrete energy spectrum with δ-like density of states[1-2]. These zero-dimensional systems can be employed for quantum device applications such as in lasers[3], single electron transistors[4], and optical memory structures[5], which promise performance improvements of the devices compared to conventional technology. Self-assembled QDs can be formed and derived by strain in highly lattice-mismatched semiconductor materials via heteroepitaxy. The coherent islands appear beyond a critical thickness of the deposited layer during Stranski-Krastanow (SK) strained layer epitaxial growth mode[6-8]. Many workers have concentrated their efforts on the study of the structureal[9-14], optical[15-19] and electronic properties[20-22] of the InAs/GaAs self-assembled QDs. However, the overall performance of devices has remained inferior to that of quantum wells (QWs) mainly because the size, shape, and composition fluctuation that occur in QDs devices result in a broad photoluminescence (PL) line width of about 40~60 meV at room temperature.

Recently, self-assembled QDs have extended the wavelength range of the InGaAs/GaAs system further into the infrared beyond 1.3 μm[15]. The InGaAs QDs have also been optimized with uniform, homogeneous and high area densities. High-power semiconductor laser diodes based on multiple InGaAs/GaAs QDs layers grown by metal-organic chemical-vapor deposition (MOCVD) technique are demonstrated[3]. However, high quality self-assembled QDs via the Stranski-Krastanow growth mode using gas-source molecular beam epitaxy (GS-MBE) still need more work to improve their uniformly in size and shape. The identification of the growth mechanisms that lead to a narrow size distribution is of great importance.

In this work, we report growth method and parameter optimization of InGaAs/GaAs self-assembled QDs, grown by GS-MBE system using migration enhanced epitaxy technique. Optical characterization is carried out by temperature-dependent PL and photoreflectance (PR) spectroscopies. Furthermore, the morphologic and structural analyses are carried out by field emission scanning electron microscopy (SEM) and atomic force microscopy (AFM).

Ⅱ.Experimental details

The samples were grown by a VG-80H GS-MBE system on n^+-GaAs (100) substrates. Samples S_1 and S_2 were made with migration enhanced epitaxy in a growth order sequence, In-Ga-As and In-As-Ga-As, respectively. The V/III ratio was 10 and the growth temperature was 500 °C. It consists of 500 nm of a GaAs buffer layer followed by 12 periods of GaAs/AlAs short period superlattice (SPS) with a thickness of 2 nm /2 nm, respectively. Then an undoped GaAs epilayer with a thickness of 50 nm is grown. An $In_{0.5}Ga_{0.5}As$ QD layer with a 10 monolayers (MLs) nominal thickness was grown on top of it and covered by 510 nm of GaAs. In order to examine the morphology and perform the structure analysis, the second InGaAs QDs layer was grown on the top layer.

The morphology structure and surface density analysis of InGaAs QDs on the top layer was performed with a SEM. The height and diameter of the QDs as well as size distribution were roughly measured by AFM on uncapped islands of InGaAs on the top layer. AFM measurements were carried out at ambient environment with a DI (Digital Instrument Inc.) Nanoscope III ® AFM (tapping mode).

Photoluminescence measurements were carried out with a 25-mW He-Ne laser at 632 nm and focused on to the sample to a spot size of 1 mm^2. The basic PR experimental setup is described in the literature[23]. The PR measurements were carried out with a 200-Walt halogen-tungsten lamp, which was dispersed by a monochromator to serve as a probe beam. A line of 543.2 nm He-Ne laser with output power of 100 μW was provided as a pumping beam. A mechanical chopper operated at a frequency of 265 Hz to modulate the pumping light. The optical signal of the reflected light from the sample was detected by a liquid-nitrogen-cooled InAs detector.

Ⅲ. Results and discussion

Fig. 1(a) and 1(b) show the SEM images of the InGaAs QDs for samples S_1 and S_2. The images present the uniform QDs and dome (lens-like) QD shape as well as the particle size. The area density of the QDs for S_1 and S_2 are $2.0x10^{10}$ cm^{-2} and $1.8x10^{10}$ cm^{-2}, respectively. The AFM images of samples S_1 and S_2 are shown in Fig. 2(a) and 2(b). The average of QD height and base length (diameters) for S_1 and S_2 are 15 nm × 17 nm and 6 nm × 24 nm, respectively. The area densities of the QDs for S_1 and S_2 are 4.8×10^{10} cm^{-2} and 1.9×10^{10} cm^{-2}, respectively. However, the area density of QDs is the same order of magnitude ($\sim1.0\times10^{10}$ cm^{-2}) but the magnitude is a little different. It might be due to the probing of different area of the samples using the SEM and AFM microscopes. The results confirm that the uniformity of QDs on S_1 is better than S_2, but the size of QD on S_1 is larger than S_2. It seems to be that the growth sequential ordering of In-Ga-As could improve better quality of QDs than In-As-Ga-As.

The PL spectra of un-etched samples S_1 and S_2 measured at low temperature (11 K) are shown in Fig. 3(a). Spectra at same temperature of samples S_1 and S_2 after etching the top-layer QDs are shown in Fig. 3(b).

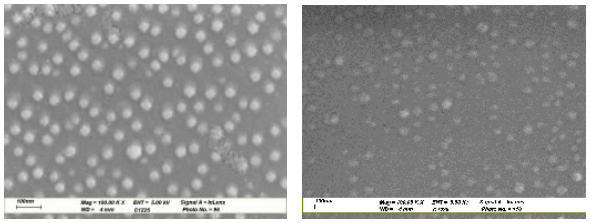

Fig. 1 SEM images of InGaAs/GaAs QDs samples S_1(a) and S_2(b).

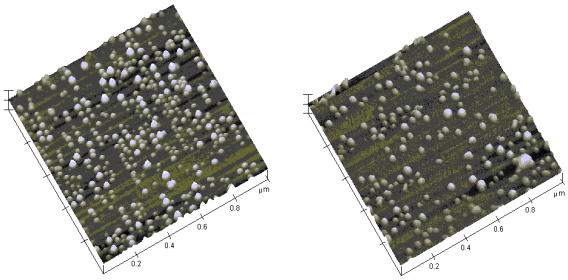

Fig. 2. AFM images of InGaAs/GaAs QDs samples S_1(a) and S_2(b).

Fig. 3 Low temperature PL spectra of InGaAs/GaAs QDs with difference growth sequence ordering using migration enhanced technique for sample S_1(In-Ga-As) and S_2 (In-As-Ga-As). (a). Before removing the top QDs layer. (b). After removing the top

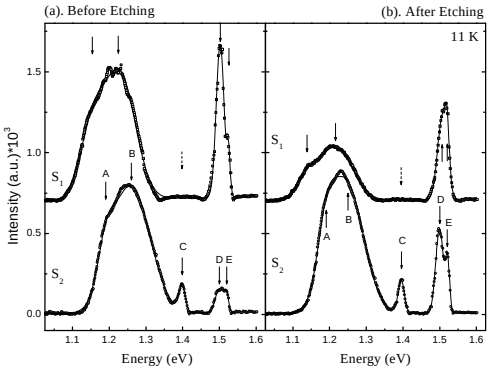

QDs layer.

The energy features on PL for etching and un-etching cases spectra are a little different, but the major energy features are presented on both figures. The optical transitions are labeled by symbols A, B, C, D and E, and marked by arrows on peak positions shown in the figures. Before etching the top-layer QDs of sample S_1, the peak energy values E_A and E_B are 1.15 eV and 1.23 eV, respectively. The corresponding broadening parameters are 34 meV and 42 meV. After etching, the energy peak values E_A and E_B are 1.14 eV and 1.22 eV with broadening parameters 27 meV and 46 meV. The results show that the shape and particle size as well as the transition energy are slightly different. For un-etched sample S_2, the energy peak values E_A and E_B are 1.19 eV and 1.25 eV with corresponding broadening parameters 23 meV and 51 meV. After etching, the transition energy values E_A and E_B are 1.19 eV and 1.25eV with corresponding line-width parameters 23 meV and 47 meV. Unlike sample S_1, the results of S_2 show that the energy transitions and broadening parameters are almost the same. It means the growth morphology of the QDs on top layer was less affected by the QDs grown on bottom layer covered with a 510-nm GaAs spacer. The average volume (particle size, height ×diameter^2) of the QDs on samples S_1 and S_2 measured with AFM are roughly to 4.3×10^3 nm^3 and 3.5×10^3 nm^3. Thus the average particle size on sample S_1 is larger than that on sample S_2. The results also show that transition energy of S_2 is higher than S_1. We propose that the E_A and E_B energy features are attributed to the optical transition of the ground state of the QDs with two kinds of QDs particle ensembles. The reason will be discussed in following next three paragraphs.

The energy value of the C peak is about 1.40 eV but is not present on sample S_1. It is reasonable and consistent that sample S_1 grew with higher average area density and larger average volume of the QD particles than those of sample S_2. The energy feature of the InGaAs wetting layer on InGaAs/GaAs QD specimens are reported in the literature[22]. Therefore, the E_C peak originates from the wetting layer. However, the peak disappears on sample S_1 due to the larger nano-particles (i.e. QDs). The energy value of the D and E peaks are about 1.50 eV and 1.52 eV for samples S_1 and S_2 without or with etching process. The broadening parameters are different and varied from 4 to 15 meV depending on the sample and etching process. The lower energy peak E_D (1.50 eV) is attributed to the buffer layer and the higher energy peak E_E (1.52 eV) originates from the GaAs cap layer. The fitted results are

summarized and listed in Table 1.

Table 1. Summary of the fitted results from PL spectra at low temperature (11 K). Symbols are denoted with UE (un-etched) and E (etched). The transition energy values in eV and broadening parameters in meV units.

Sample		Transition energy features									
		E_A	Γ_A	E_B	Γ_B	E_C	Γ_C	E_D	Γ_D	E_E	Γ_E
S_1	UE	1.15	34	1.23	42	—	—	1.50	11	1.52	4
	E	1.14	27	1.22	46	—	—	1.51	14	—	—
S_2	UE	1.19	23	1.25	51	1.40	8	1.50	11	1.52	6
	E	1.19	23	1.25	47	1.40	8	1.50	15	1.52	6

PR spectra carried out at room temperature and low temperature are shown in Fig. 4(a) for sample S_1 and Fig. 4(b) for sample S_2 .The energy features are fitted by the third derivative function form (TDFF) with a Lorentzian line shape[24]. The energy peaks are labeled with the symbols C, D, and E corresponding to Fig. 3 and marked by an arrow notation on the peak position. Two energy values (D, E) fitted by a χ^2 fitting method of TDFF Lorentzian line shape are 1.420 (1.423) eV and 1.439 (1.440) eV at room temperature for samples S_1 (S_2), respectively. The results summary is shown in Table 2. The energy features (D, E) are attributed to the buffer and cap layers of GaAs. The peak C originates from the InGaAs wetting layer. PR spectra measured at low temperature (50 K) display more energy features which are contributed to the InGaAs wetting layer, GaAs cap and buffer layers. These energy features could not be well fitted to the room-temperature PR spectra. The line shape of PR spectra also changed severely due to temperature cooling down below 50 K. PR spectra might provide more information after detailed line shape analysis which includes strain on GaAs layer. This needs more study in the future.

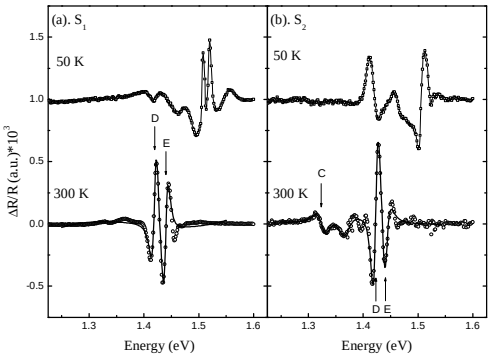

Fig. 4 PR spectra of InGaAs/GaAs QDs measured at room temperature (300 K) and low temperature (50 K) for samples (a) S_1 and (2) S_2.

Table 2. Summary of TDFF fitted results from room-temperature PR spectra of un-etched samples S_1 and S_2. Energy values in eV and broadening parameters in meV units.

Sample	Transition energy features

	E_C	Γ_C	E_D	Γ_D	E_E	Γ_E
S_1	—	—	1.420	9	1.439	10
S_2	1.326	18	1.423	9	1.440	11

The transition energies measured with PL of low energy portions (E_A and E_B) are plotted as a function of temperature for samples S_1 and S_2 (before etching) are shown in Fig. 5. The trends observed in E_A (InGaAs QDs), E_B (InGaAs QDs) and E_C (InGaAs wetting layer) are different due to the temperature-dependent band-gap of InAs and GaAs materials. Because the wetting layer is an ultra thin InGaAs/GaAs quantum wells, the curve trend on the temperature will follow that of the host material of GaAs. However, the InGaAs QDs will be related to temperature behavior characteristic of the InAs and GaAs materials. The optical properties of the InGaAs QDs and wetting layer were studied with the fitting parameters using Varshni's equation[24]. The summary of the fitting results are listed in Table 3. The argument of the peak identification was supported by this result. A slight abnormal behavior of the inverted “S-curve” shape on temperature-dependent transition energies measured by PL spectra was observed. It has been explained by the carrier localization on potential minimum of In-rich island[24]. This effect could be studied by time-resolved PL spectroscopy in the future.

Ⅳ. Conclusion

Temperature-dependent PL and PR experiments were performed and the optical properties of

Fig. 5 Transition energies in the low energy portion measured by PL experiments are plotted as a function of temperature.

Table 3. Results summary of the fitted parameters using Varshni’s equation to fit the temperature-dependent transition energy.

Energy peak	Parameters	Sample		Notes
		S_1	S_2	
A	E (eV)	1.144	1.192	QDs[1]
	α ($\times 10^{-4}$eV/K)	-5.9	-8.8	
	β (K)	243	254	
B	E (eV)	1.221	1.266	QDs[2]
	α ($\times 10^{-4}$eV/K)	-8.7	-8.9	
	β (K)	259	245	
C	E (eV)	—	1.401	WL
	α ($\times 10^{-4}$eV/K)	—	-3.5	
	β (K)	—	253	

InGaAs/GaAs self-assembled QDs grown by GS-MBE system were studied. Samples of two growth ordering sequences of the adatom, In-Ga-As andIn-As-Ga-As, are explored and characterized with temperature-dependent transition energy spectra and identified two kinds of InGaAs/GaAs QDs ensembles which are originated from two different indium composition fluctuation. The major energy

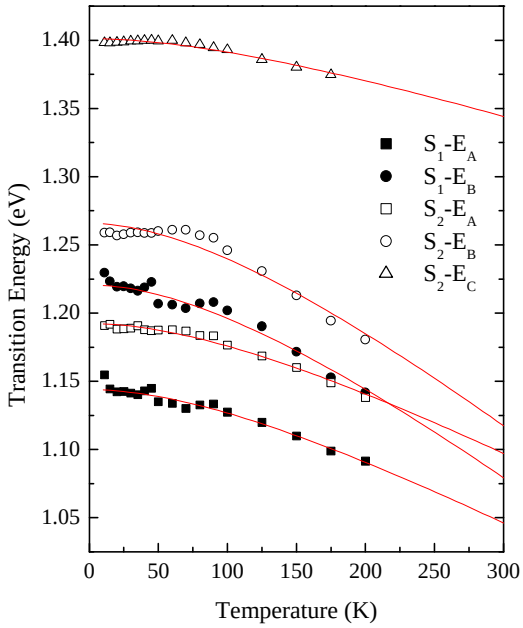

peaks display on PL and PR spectra were identified and interpreted. An abnormal behavior of the inverted “S-curve” shape presented on temperature-dependent transition energy due to carrier localization were also observed.

References

1. D. Bimberg, M. Grundmann, and N. N. Ledenstov, *Quantum Dot Heterostructures* (Wiley, Chichester, 1998).
2. Y. Toda, O. Moriwaki, M. Nishioka, and Y. Arakawa, Phys. Rev. Lett. **82**, 4114 (1999).
3. F. Heinrichsdorff, Ch. Ribbat, M. Grundmann, and D. Bimberg, Appl. Phys. Lett. **76**, 556 (2000).
4. N. Yokoyama, S. Muto, K. Imamura, M. takatsu, T.Mori, Y. Sugiyama, Y. Sakuma, H.Nakao, and T. Adachihara, Solid State Electron. 40, 505 (1996).
5. G.Yusa and H. Sakaki, Appl. Phys. Lett. 70,345 (1997).
6. I. N. Stranski and L. Krastanow, Akad. Wiss. Lit. Mainz Abh. Math. Naturwiss. **K1 IIb 146**, 797 (1939).
7. D. Leonard, K. Pond, and P. M. Petroff, Phys. Rev. B **50**, 11687 (1994).
8. D. Leonard, M. Krishnamurthy, C. M. Reaves, S. P. Denbaars, and P. M. Petroff, Appl. Phys. Lett. **63**, 3203 (1993).
9. L. Goldstein, F. Glas, J. Y. Marzin, M. N. Charasse, and G. Le Roux, Appl. Phys. Lett. **47**, 1099 (1985).
10. S. Guha, A. Madhukar, and K. C. Rajkumar, Appl. Phys. Lett. **57**, 2110 (1990).
11. J. M. Moison, F. Houzay, F. Barthe, and L. Leprince, E. Andre, and D. Vatel, Appl. Phys. Lett. **64**, 196 (1994).
12. A. Tackeuchi, Y. Nakata, S. Muto, Y. Sugiyama, T. Inata, and N. Yokoyama, Jpn. J. Appl. Phys. **34**, L 405 (1995).
13. P. B. Joyce, E. C. Le Ru, T. J. Krzyzewski, G. R. Bell, R. Murray, and T. S. Jones, Phys. Rev. B **66,** 75316 (2002).
14. A. A. Darhuber, V. Holy, J. Stangl, G. Bauer, A. Krost, F. Heinrichsdroff, M. Grundmann, D.

Bimberg, V. M. Ustinov, P. S. Kop'ev, A. O. Kosogov, and P. Werner, Appl. Phys. Lett. **70**, 955 (1997).

15. R. P. Mirin, J. P. Ibbetson, K. Nishi, A. C. Gossard, and J. E. Bowers, Appl. Phys. Lett. **67**, 3795 (1995).
16. S. Farfad, R. Leon, D. Leonard, J. L. Merz, and P. M. Petroff, Phys Rev. B **52**, 5752 (1995).
17. J. M. Garcia, G. Medeiros-Ribeiro, K. Schmidt, T. Ngo, J. L. Feng, A. Lorke, J. Kotthaus, and P. M. Petroff, Appl. Phys. Lett. **71**, 2014 (1997).
18. Q. D. Zhuang, J. M. Li, H. X. Li, Y. P. Zeng, L. Pan, Y. H. Chen, M. Y. Kong, and L. Y. Lin, Appl. Pys. Lett. **73**, 3706 (1998).
19. L. Chu, M. Zrenner, M. Bichler, G. Böhm, and G. Abstreiter, Appl. Phys. Lett. **77**, 3944 (2000).
20. P. W. Fry, *et al*, Phys. Rev. Lett. **84**, 733 (2000).
21. J. J. Finley, M. Skalitz, M. Arzberger, A. Zrenner, G. Böhm and G. Abstreiter, Appl. Phys. Lett. **73**, 2618 (1998).
22. L. Chu, M. Zrenner, G. Böhm, and G. Abstreiter, Appl. Phys. Lett. **76**, 1944 (2000).
23. F. H. Pollak, in *Handbook on Semiconductors*, edited by Balhanski (North-Holland, New York, 1993), Vol. 2.
24. K. L. Teo, J. S. Colton, P. Y. Yu, E. R. Weber, M. F. Li, W. Li, K. Uchida, H. Tokunaga, N. Akutsu, and K. Matsumoto, Appl. Phys. Lett **73**, 1697 (1998).